JOURNAL OF APPLIED ELECTROCHEMISTRY 4 (1974) 25–48

Blackening in yttria stabilized zirconia due to cathodic processes at solid platinum electrodes

R. E. W. CASSELTON

International Research and Development Ltd., Newcastle upon Tyne, NE6 2YD

Received 23 May 1973.

The DC cathodic voltage current density (V–J) characteristics at the contact between a solid disc Pt—13% Rh electrode and yttria stabilized zirconia (YZr) electrolyte were investigated to evaluate the conditions under which blackening occurred in the anionic conductor. Polycrystalline and single crystal samples have been studied using oxygen-argon mixtures between 10^0 and 10^{-3} atm oxygen and at temperatures in the range 800 to 1450°C. It is shown that the rate determining step of the overall cathodic reaction, $O_2(g)+2V\ddot{o}+4e' \rightarrow 2O_O^x$ under low field, ohmic conditions is the first electronation step, but true activation polarization at higher fields is masked by mass transfer limitations. The limiting current density in the polycrystalline material was directly proportional to the oxygen partial pressure ($J_L \propto P_{O_2}$) whereas at low temperatures, below 1000°C, $J_L \propto P_{O_2}^{\frac{1}{4}}$ in the single crystal.

The former behaviour is attributed to a flux limit in the ambient oxygen gas, whereas the $J_L \propto P_{O_2}^{\frac{1}{4}}$ regime is believed to be a consequence of molecular dissociation, coupled with surface exchange, onto the mobile interfacial layer. It is further shown that blackening is a consequence of thermionic emission of electrons across the cathodic interface into anion vacancy traps and the cathodic V–J characteristics of the blackened material saturate to obey a $J \propto V^2$ law above about 2 V, indicative of a space charge limited current. A tentative model is proposed.

1. Introduction

The stabilization of zirconia into the cubic fluorite phase by the substitution of an aliovalent oxide, such as yttria, arises from the creation of oxygen anion vacancies, which enable the material to conduct ionically above about 1000°C [1].

At low fields, the mass transfer of anion vacancies is presumably sustained by redox reactions at the metal/electrolyte/oxygen interface. However, it is well known that such stabilized zirconias acquire a characteristic black colour, initiating at the cathode, when subject to a large current density. As a result the conduction is enhanced due to an increased electronic contribution, Jacquin [2].

Etsell and Flengas [3] have pointed out the confusion in the literature (Table 1) concerning the rate limiting mechanisms responsible for the onset of blackening, and support the view of Brook *et al.* [4] that the inconsistencies demonstrate the important influence of electrode structure on reproducibility. It must be emphasized that, without exception, all previous experimentalists have measured potentials directly across the cell and assumed that anodic effects are small compared to the cathodic polarization.

The present work arose out of a study of the conduction mechanisms in yttria stabilized zirconia (YZr) and included an evaluation of the onset of blackening under conditions appropriate to an open-cycle MHD system [12]. The low field conduction in YZr has been shown to

Table 1. Summary of previous work on electrolysis of solid electrolytes using oxygen-based gas mixtures

Ref.	*Electrolyte material and size*	*Electrode material and size*	*Temperature range (°C)*	*O_2-argon partial pressure range (atm)*	*$J_L \propto P_{O_2}$ Relation*	*Typical J_L values*	*Rate limiting mechanism*
[3]	10 mol % CaO:ZrO_2, butt tube end, 1 cm diam. ×0·4 cm thick	Porous Pt black fired 600–700°C, ~1 cm diam.	700–1100	10°–10^{-3}	$J_L \propto P_{O_2}$	2×10^{-2}A cm^{-2} at 6×10^{-3} atm, 1000°C.	Diffusion of gaseous O_2 molecules through Pt pores
[4]	15 mol % CaO:ZrO_2, disc 0·2 cm^2 × 0·07 cm thick	(a) Pt foil, (b) non-porous sputtered Pt (c) Pt paste of various porosities, ~0·2 cm^2	500–700	10°–10^{-3}	$J_L \propto P_{O_2}^{\frac{1}{2}}$	8×10^{-4}A cm^{-2} at 2×10^{-1} atm, 560°C.	Diffusion of O atoms through Pt electrode
[5]	15 mol % CaO:CeO_2, size not specified	Porous Pt paste pre-treated at high anode currents, ~0·4 cm^2	600–1000	10°	—	—	Pt-O interaction
[6]	10 mol % Y_2O_3:ZrO_2, bars either 0·1 × 0·1 × 1·2 cm or 0·1 × 0·3 × 0·4 cm.	(a) Dense Pt paste, fired 1400°C. (b) Semi-porous sputtered Pt, covering end face area	400–800	10°–$1{\cdot}5\times10^{-5}$	—	—	Either (a) dissociation of molecular oxygen or (b) electron transfer step
[7]	12 mol % Sc_2O_3:ZrO_2, cylinder 1·5 × 0·3 cm diam.	Pt paste	800–1000	10°–2×10^{-1}	—	—	Mass transport in the gas phase
[8]	12·5 mol % CaO:ZrO_2 disc	Point Pt electrode	700–1200	2×10^{-1}–2×10^{-4}	$J_L \propto P_{O_2}^{\frac{1}{2}}$	5×10^{-6}A at $1{\cdot}3\times10^{-1}$ atm, 870°C (area of point electrode not specified)	Diffusion of O atoms through the adsorbed phase
[9]	10 mol % CaO:ZrO_2, disc ~0·2 cm^2.	Porous Pt fired 800°C, <0·01 cm^2	560	10°–10^{-3} (O_2–N_2)	$J_L \propto P_{O_2}^{\frac{1}{2}}$	10^{-4}A cm^{-2} at 4×10^{-3} atm, 560°C.	Diffusion of O atoms through the Pt electrode
[10]	10 mol % Y_2O_3:ZrO_2 disc	Porous $PrCoO_3$, 0·013 cm thick, diam. small compared to disc (Ni anode)	800–1200	5×10^{-1}–5×10^{-2}	$J_L \propto P_{O_2}$	9×10^{-1}A cm^{-2} at 5×10^{-2} atm, 1000°C.	Mass transport in the gas phase
[11]	15 mol % Y_2O_3:ZrO_2, cylindrical bar 1·5 cm × 0·7 cm diam.	Pt disc, 0·02 cm × 0·4 cm diam.	1400	2×10^{-1}	—	8×10^{-1}A cm^{-2} at 2×10^{-1} atm, 1400°C.	Diffusion of gaseous O_2 molecules through the interface

be entirely ionic [13]. This paper examines the equilibrium voltage current density (V–J) characteristics of both polycrystalline and single crystal YZr sandwiched between solid Pt-Rh electrodes.

2. Experimental

Details for the preparation of 95% dense polycrystalline 12 mol % YZr cylindrical samples and of a multiprobe conductivity apparatus have been given elsewhere [14]. Single crystal samples of 8·3 mol % YZr, prepared by arc fusion under nitrogen*, were annealed at 1500°C in oxygen to remove preparative substoichiometry and, as with the polycrystalline samples, showed no X-ray evidence of a monoclinic phase.

For the present work DC V–J curves were obtained by monitoring the potential between a solid Pt-13 wt % Rh electrode and an adjacent probe inserted into a hole drilled diametrically into the sample to one-third of its diameter; the electrode-probe distance being of the order of 0·2–0·3 cm. The disc electrodes of diameter 0·8 cm and thickness 0·2 cm were attached to the samples by a Pt paste intermediary.† They covered three-quarters of the end face of polycrystalline cylindrical bars. The limited size of available single crystals necessitated complete coverage of their cylindrical end faces. In all cases the electrode-electrolyte assembly was fired to 1500°C and thermally cycled before use. Except where mentioned, all measurements were DC, made in oxygen-argon gas mixtures at a total room temperature pressure of 1 atm, and 1 l min^{-1} gas flow rate. Equilibrium conditions were attained prior to all measurements, in respect of potential, ambient oxygen atmosphere and temperature.

3. Results

3.1. *Equilibrium potential distribution across samples*

Figs. 1(a–c) show a sequence of typical equilibrium DC potential distribution curves obtained at 1380°C on polycrystalline 12 mol % YZr for increasing current densities and oxygen partial pressure. These curves are corrected for thermoelectric, but not for contact e.m.f.'s, which could only be evaluated under equilibrium zero current conditions and which were therefore difficult to obtain when blackening was present. Corrections for contact e.m.f.'s, which could be estimated for unblackened samples, revealed negligible electrode polarization, irrespective of oxygen content, under conditions corresponding to the ohmic α region of Fig. 2a. The bulk linearity and reproducibility confirm that there is equilibrium between probe and electrolyte which is uninfluenced by the electrochemical potentials of electrons in the latter.

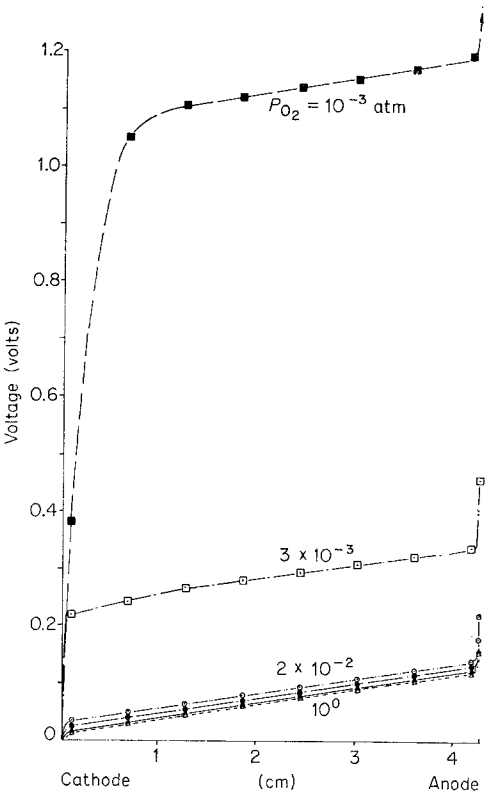

Fig. 1a. Potential distribution at 1380°C in 12 mol % Y_2O_3:ZrO_2 at $1{\cdot}29 \times 10^{-3}$ A cm^{-2} for various oxygen partial pressures.

Samples quenched from 1380°C, after reaching equilibrium under the stated conditions of current density and oxygen partial pressure in Fig. 1c, showed that the space charge regions

* Obtained from Spicers Ltd., Cheltenham, England.
† Johnston-Matthey type 75N containing a small amount of lead borosilicate flux.

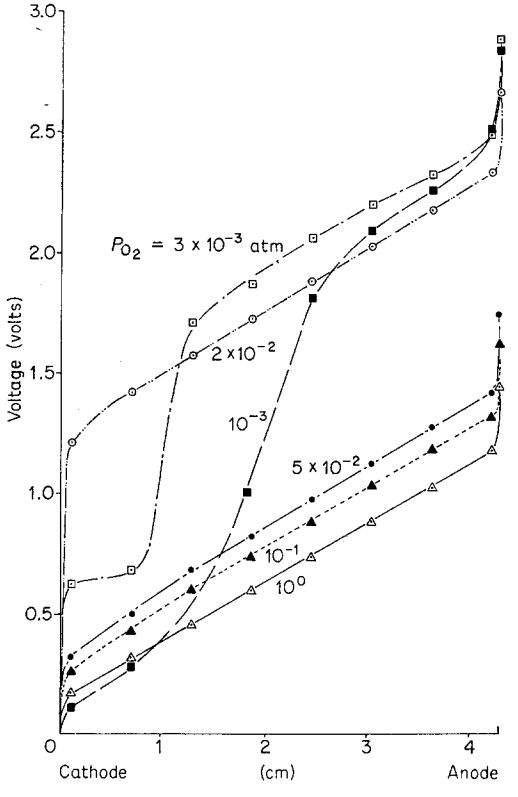

Fig. 1b. Potential distribution at 1380°C in 12 mol % Y_2O_3:ZrO_2 at $1{\cdot}29 \times 10^{-1}$ A cm^{-2} for various oxygen partial pressures.

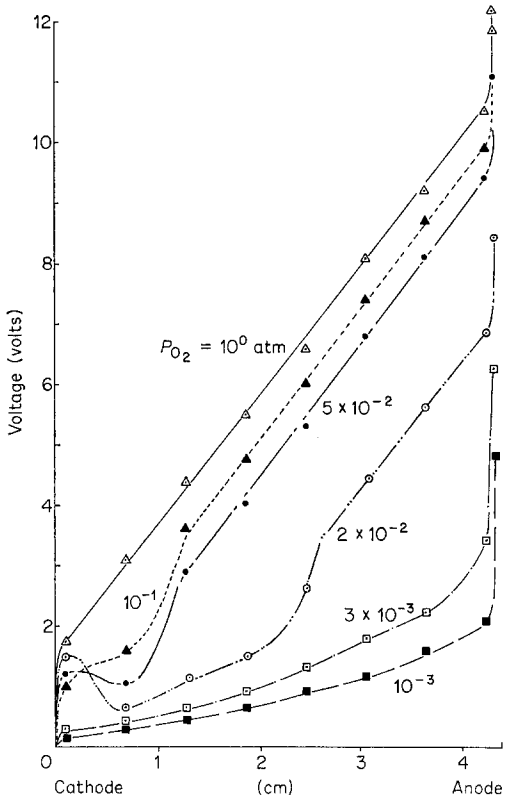

Fig. 1c. Potential distribution at 1380°C in 12 mol % Y_2O_3:ZrO_2 at 1·29 A cm^{-2} for various oxygen partial pressures.

indicated by the potential distribution curves are due to the formation of a tongue-shaped blackened zone at the cathode.

The general characteristics of Fig. 1 apply also to single crystal 8·3 mol % YZr, but significantly longer equilibration times were necessary compared to the polycrystalline material; as long as 1 h compared to 20 min in impure argon at 1400°C and 10^{-3} A cm^{-2}.

3.2. *Cathodic voltage-current density characteristics*

The equilibrium DC *V–J* characteristics at both the cathode and anode are shown in Fig. 2; these were obtained on polycrystalline 12 mol % YZr at 1380°C as a function of ambient oxygen partial pressure. The voltage V is the total potential measured between the electrode and neighbouring probe, and includes contributions from zero current potentials, bulk electrolyte resistance and any overpotential that may be present. Accordingly $V = IR_b + \eta_o + \eta_p$, where R_b is the bulk specimen resistance, η_o is the zero current reversible potential and η_p is the polarization overpotential which may itself include charge transfer (activation $-\eta_a$) and mass transfer (concentration $-\eta_c$) terms. It is considered from the position of the monitoring probe that the *V–J* curves of Fig. 2 are the result of true electrode processes, independent of oxygen diffusion effects from the cylindrical sample surface which may control the shape of the blackened zones. Of two specimens quenched from points A and B on the cathodic trace (Fig. 2a) for $2{\cdot}2 \times 10^{-3}$ atm ambient, only that sample quenched from B exhibited slight discolouration around the cathode interface after stripping away the electrode; the turnover point C therefore corresponded to onset of blackening.

Of particular interest is the curve obtained for a CO_2 atmosphere which does not show the

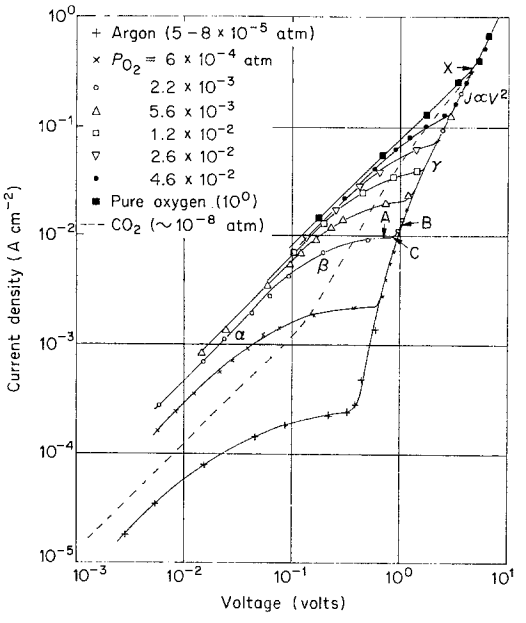

Fig. 2a. Cathodic current density–voltage characteristic of 12 mol % Y_2O_3:ZrO_2 at 1380°C for different oxygen partial pressures. α = ohmic region, β = mass transfer limited region, γ = blackened zone. A, Band C, see text, section 3.2. X = onset of blackening in CO_2 and pure oxygen.

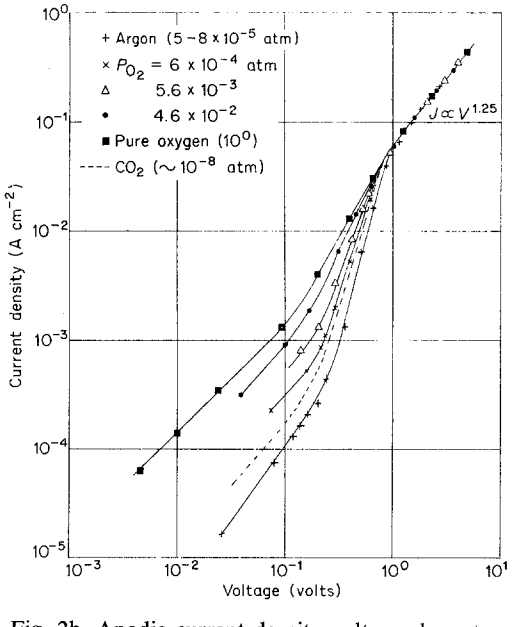

Fig. 2b. Anodic current density–voltage characteristic of 12 mol % Y_2O_3:ZrO_2 at 1380°C for different oxygen partial pressures.

cathodic polarization characteristics exhibited by samples in gas mixtures containing oxygen. The low field bulk conductivity was found invariant with respect to both CO_2 and O_2-based atmospheres. Quenching experiments indicated that samples in CO_2 atmospheres do not exhibit blackening until X is reached on Fig. 2a, this being similar to the operative condition required for onset of blackening in pure oxygen. The similarity between the low field cathodic and anodic V–J curves for CO_2 is striking, with identical, $J \propto V^{1.25}$, behaviour above about 6×10^{-2} A cm^{-2} at 1380°C.

The V–J characteristics for single crystal 8·3 mol % YZr were similar to polycrystalline material, except, as previously noted, the attainment of equilibrium was much more sluggish. Additionally, the transition to the blackened state (corresponding to C in Fig. 2a) was much less well-defined, exhibiting a more rounded trace.

The three regions of interest α, β, and γ in the cathodic trace of Fig. 2a are considered in the following section, the anodic phenomena having no relevance to the problem of blackening in YZr.

3.2.1. *The low field ohmic region* (α). Since the low field potential distribution in Fig. 1a shows that the bulk conductivity is pressure invariant, the relative shift of the V–J traces in the ohmic region of Fig. 2a with oxygen partial pressure is a consequence of the zero current reversible potential.

This lack of pressure dependence, however, was only found if the ambient gas flow was from anode to cathode, corresponding to the direction of anion vacancy transport. A weak but well-defined oxygen partial pressure dependence was exhibited if the vacancy transport and gas flow were not in complementary directions [15].

Fig. 3 indicates the trend of the total low field DC cathodic resistance (R_t) as a function of oxygen partial pressure (P_{O_2}) and temperature (T), from the ohmic V–J data. R_t includes two contributions; one due to the bulk resistance R_b of the electrolyte between cathode and measuring probe (independent of gas pressure) while the polarization resistance R_p, contributed by both activation and mass transfer effects [16], is derived in Appendix A (Equations A7 and A10):

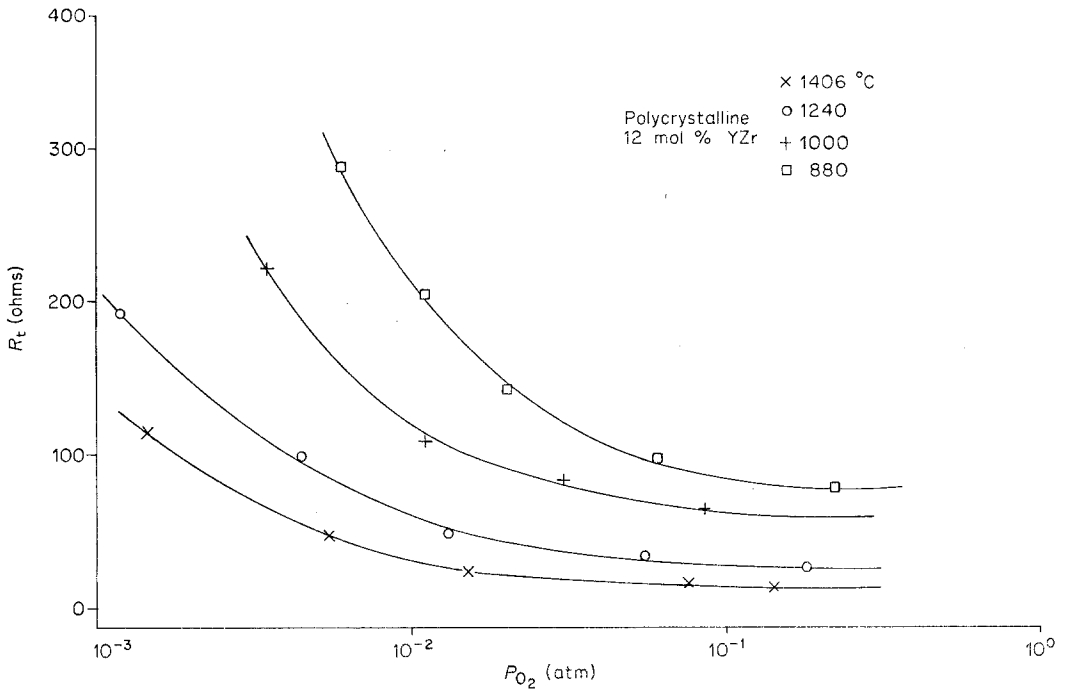

Fig. 3. The low field ohmic cathodic resistance (R_t) as a function of oxygen partial pressure and temperature.

$$R_t = R_b + R_p = R_b + \frac{1}{4\pi R^2 \beta}\left(\frac{1}{J_0} + \frac{1}{J_L}\right) \tag{2}$$

$$= R_b + \frac{1}{4\pi R^2 \beta}\left(\frac{1}{\bar{K}_0 c_g^n \exp -\beta(\bar{\alpha}\varepsilon_0 + \Delta G_0^{\#})} + \frac{1}{J_L}\right)$$

where the ambient oxygen gas concentration $c_g = \frac{1}{k}\left(\frac{10^6 P_{O_2}}{T}\right) \text{cm}^{-3}$ from kinetic theory and $\beta = (kT)^{-1}$. The bracketed terms arise respectively from activation and mass transfer contributions. If mass transfer is negligible ($J_L \gg J_0$) a plot of log dR_t/dP_{O_2} versus log $\bar{P}_{O_2}$ would give a constant slope of $(1+n)$ independent of T. Fig. 4 shows that this is the case. The dotted curves in Fig. 4 for $T = 1000$ and 1406°C show the consequences of correcting for the experimentally deduced limiting current density J_L, and indicate that a small mass transfer contribution exists. Analysing the corrected data gives $n = 0{\cdot}8_0$. The ordinate values $I_{\bar{P}=10^{\circ}}$ when plotted as log $(T^{-(1+n)} I_{\bar{P}=10^{\circ}})$ v T^{-1} gives a good straight line from which $(\bar{\alpha}\varepsilon_0 + \Delta G_0^{\#}$:) and $\bar{K}_0$ are estimated as $-0{\cdot}315$ eV and $2{\cdot}9 \times 10^{-18}$ respectively. Referring back to Equation A7 allows the exchange current density to be calculated; this is summarized in Table 2 with J_L for comparison, and it is apparent that they become comparable at low temperatures.

3.2.2. *The concentration polarization region* (β) The intermediate transition from the ohmic to blackened states exhibits a characteristic representative of a mass transfer limited process, as in electrochemical reduction phenomena. Accepting this starting point, the assumption of negligible charge transfer polarization requires that $J_0 \gg J_L$, which is contrary to Table 2, and, as Fig. 5 shows, the experimental data for the concentration overvoltage (η_c) in the β region of Fig. 2a do not obey the elementary Nernst diffusion limit relation [16]:

$$\eta_c = \frac{1}{4\beta} \ln\left(\frac{J_L}{J_L - J}\right), \quad (J_0 \gg J_L) \tag{3}$$

The nature of the slopes and non-zero intercepts in Fig. 5 clearly indicate that the assumption of negligible charge transfer polarization is invalid. The theory developed in Appendix B leads to

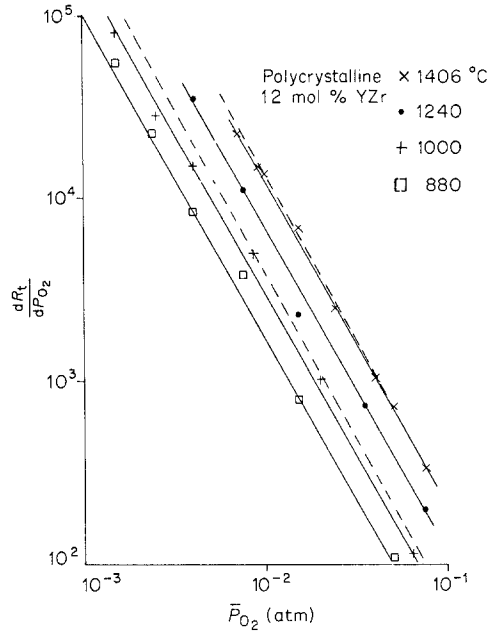

Fig. 4. Plot of the incremental gradient (dR_t/dP_{O_2}) from Fig. 3 as a function of average oxygen partial pressure ($\bar{P}_{O_2}$). The dotted curves show the influence of correction for mass transfer contribution according to Equation (A10).

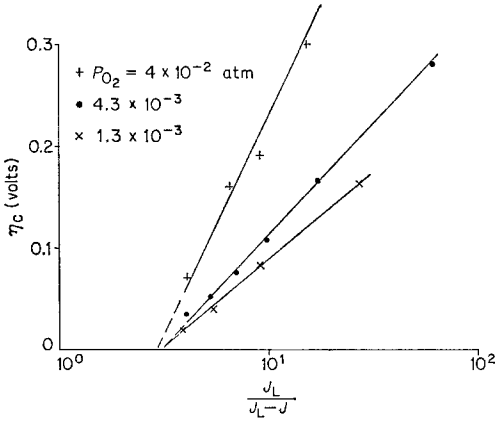

Fig. 5. Plot of the Nernst relation, Equation 3, for polycrystalline 12 mol % Y_2O_3:ZrO_2 at 1280°C.

the general overpotential-current density relation ($J>0$, $\eta<0$ for a cathodic reaction):

$$J = H\left(1-\frac{J}{J_L}\right)\exp-\alpha'\beta\eta_t \qquad (4)$$

where H is a constant (usually equated to the exchange current density J_0 for strong activation), α' is an appropriate transfer coefficient and η_t is the total, measured overpotential related to its charge transfer and concentraton components by:

$$\alpha'\eta_t = \alpha\eta_a+\eta_c, \qquad (5)$$

α being the true charge transfer coefficient.

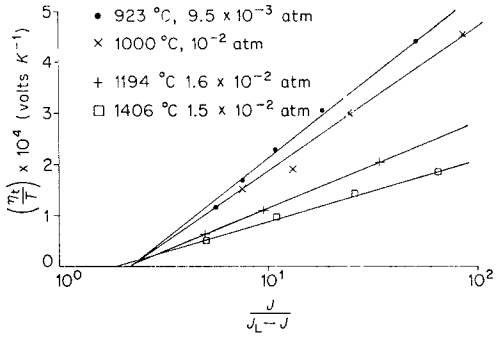

Fig. 6. Equation 4a plotted as a function of temperature for oxygen partial pressures around 10^{-2} atm.

Fig. 6 is a plot of Equation 4 in the rearranged form:

$$\frac{|\eta_t|}{T} = \frac{k}{\alpha'}\left[\ln\frac{J}{J_L-J}+\ln\frac{J_L}{H}\right] \qquad (4a)$$

for $P_{O_2}\approx10^{-2}$ atm and shows the β region of Fig. 2a to obey this relation well. It is apparent that the ratio H/J_L is approximately constant for the stated oxygen partial pressure and that α' is strongly temperature dependent. Consequently all the experimental data were computer fitted to Equation 4 and the parameters J_L, H/J_L and α' extracted. The limiting overpotential η_L corresponding to initiation of blackening at point C on Fig. 2a was also estimated. The small overpotential existing above about 10^{-1} atm precluded reliable assessment of the parameters, and since CO_2-based atmospheres led to a different polarization phenomena, valid data were only available over a relatively narrow range of oxygen partial pressures between 10^{-1} and 6×10^{-4} atm. However, such curves as Fig. 2a were obtained for single crystal and polycrystalline YZr over a range of temperature and pressure to give information on the parametric dependence of these variables.

Fig. 7 shows the relation of the limiting current density J_L on the ambient oxygen partial pressure at different temperatures. The single crystal

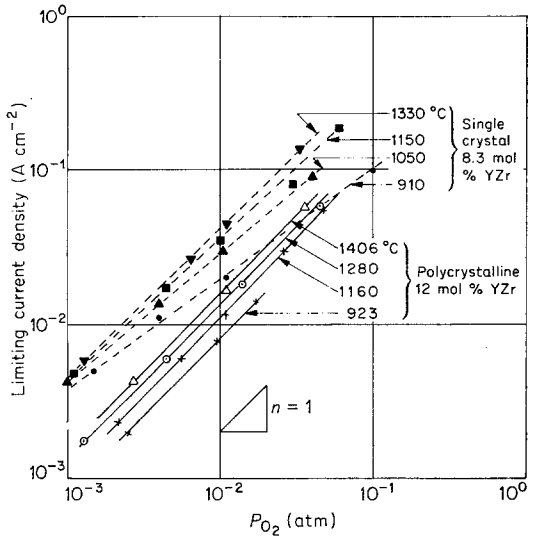

Fig. 7. Dependence of the limiting current density on oxygen partial pressure and temperature, for both polycrystalline 12 mol % Y_2O_3:ZrO_2 and single crystal 8·3 mol % Y_2O_3:ZrO_2.

data shows a $J_L \propto P_{O_2}^n$ relation; the index decreasing from unity with decreasing temperature, whilst it remained as one over the temperature range for the polycrystalline material. A Boltzmann relation for the latter (Fig. 8) can be expressed empirically as:

$$J_L = A_0 P_{O_2} T^{-\frac{1}{2}} \exp(-Q/kT) \qquad (6)$$

with $Q = 0{\cdot}26_3$ eV and $A_0 = 2{\cdot}75 \times 10^2\ AK^{-\frac{1}{2}}$ atm^{-1}. Unfortunately, the single crystal data were evaluated at only four temperatures, for which they lie in a transition zone between a high temperature $J_L \propto P_{O_2}$ and a low temperature $J_L \propto P_{O_2}^{\frac{1}{2}}$ characteristic (Fig. 9). It can be construed that the data tend towards activation energies around 1 eV and 0·3 eV at low and high temperatures respectively.

The ratio H/J_L was constant at $0{\cdot}83 \pm 0{\cdot}11$ for the single crystal and $2{\cdot}10 \pm 0{\cdot}25$ for polycrystalline 12 mol % YZr (compare intercept of Fig. 6), irrespective of partial pressure and temperature.

Fig. 10 shows the trend of the computed α' data as functions of P_{O_2} and T, the polycrystalline data exhibit a pronounced sensitivity.

3.2.3. *The blackened state* (γ) *region.* The limiting overvoltage, η_L, is a relevant parameter in that it represents the cathodic overvoltage corresponding to initiation of blackening, and Fig. 11 indicates its dependence on both temperature

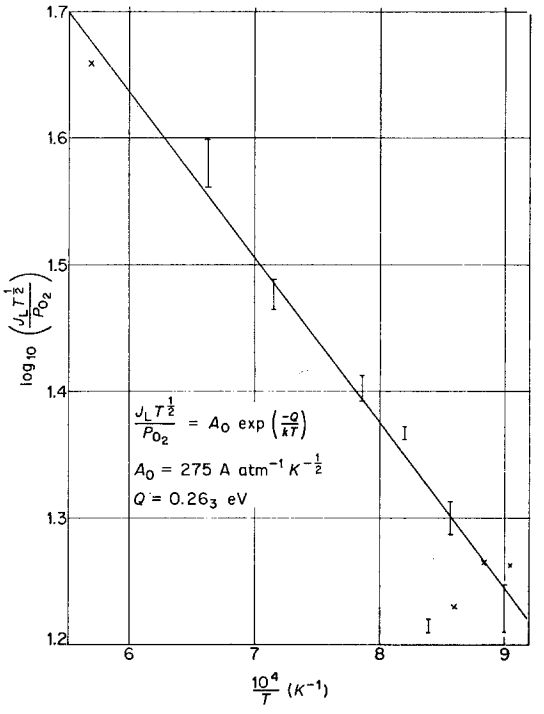

Fig. 8. Boltzmann type dependence of $\log_{10}(J_L T^{\frac{1}{2}}/P_{O_2})$ from Fig. 7 on reciprocal of absolute temperature for polycrystalline 12 mol % Y_2O_3:ZrO_2.

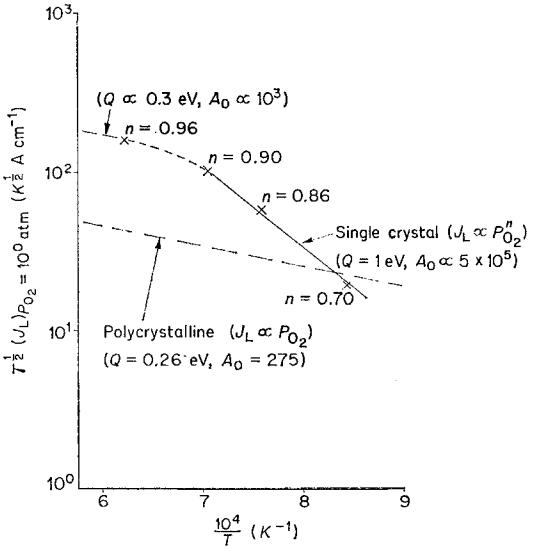

Fig. 9. The function $\log_{10}[T^{\frac{1}{2}}(J_L)_{P_{O_2}=10^0}]$ versus $1/T$ for single crystal 8·3 mol % Y_2O_3:ZrO_2. Equivalent function for polycrystalline 12 mol % Y_2O_3:ZrO_2 is included for comparison.

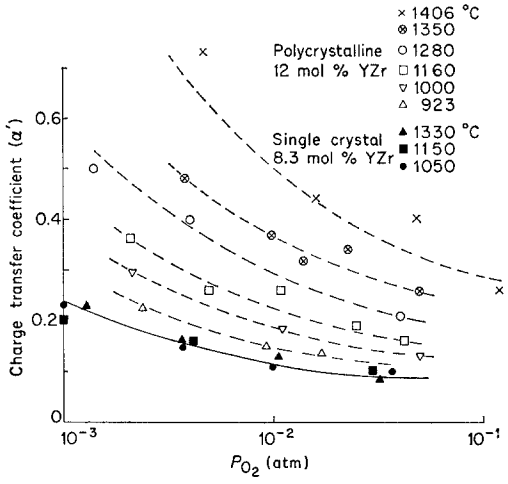

Fig. 10. Dependence of transfer coefficient α' on oxygen partial pressure and temperature.

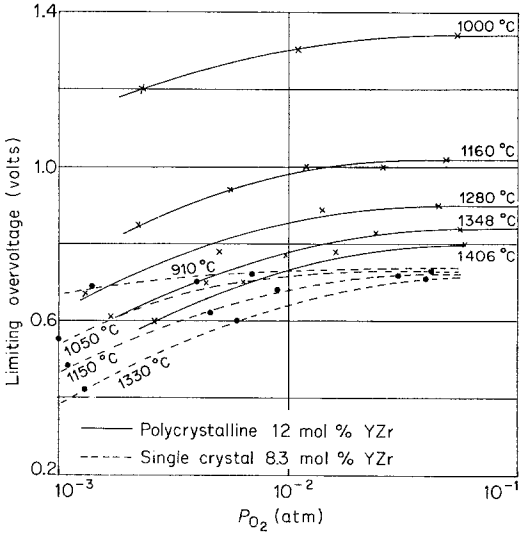

Fig. 11. Influence of oxygen partial pressure, temperature and crystallinity on the limiting over-voltage (η_L) for onset of blackening.

and crystallinity, showing that η_L approaches a constant value above about 5×10^{-2} atm. In the polycrystalline material, there is a pronounced temperature dependence of a Boltzmann type having an activation energy of $0{\cdot}24_5$ eV over the relevant range of oxygen partial pressure.

The high voltage V–J curves stabilize into a square law relation obeyed over at least a decade (Fig. 2a); a composite plot of the tangential envelope for the electronic conduction mode in polycrystalline 12 mol % YZr (Fig. 12) shows that the $J \propto V^2$ region is temperature

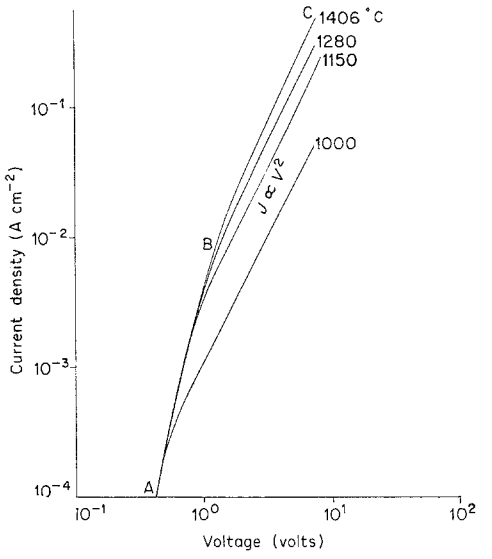

Fig. 12. Composite cathodic current density–voltage curves for the electronic conduction mode of Fig. 2a. A–B, Thermionic emission region for which a small temperature variation exists, being too insignificant for accurate plotting. B–C, space charge limited conduction.

sensitive. Identical behaviour was observed on an isolated polycrystalline sample of 17 mol % $MgO:ZrO_2$.

3.2.4. *Conductivity of blackened polycrystalline YZr.* The curve of bulk conductivity versus reciprocal of absolute temperature for a blackened polycrystalline 12 mol % YZr sample was estimated by superimposing a small 50Hz signal on a large DC maintained during the measurements to retain the blackened state. Although the sample, in purified argon, appeared completely blackened, it was found that non-reproducible results were obtained until at least 3 A cm^{-2} DC was sustained. Fig. 13 illustrates this, showing cooling curves for samples blackened at different DC current densities at 1400°C. An activation energy of 0·2 eV was deduced for the saturated condition, compared to about 0·7–0·9 eV for the stoichiometric material [13].

4. Discussion

4.1. *Introduction*

Table 1 shows that earlier work may be classified according to the derived influence of oxygen

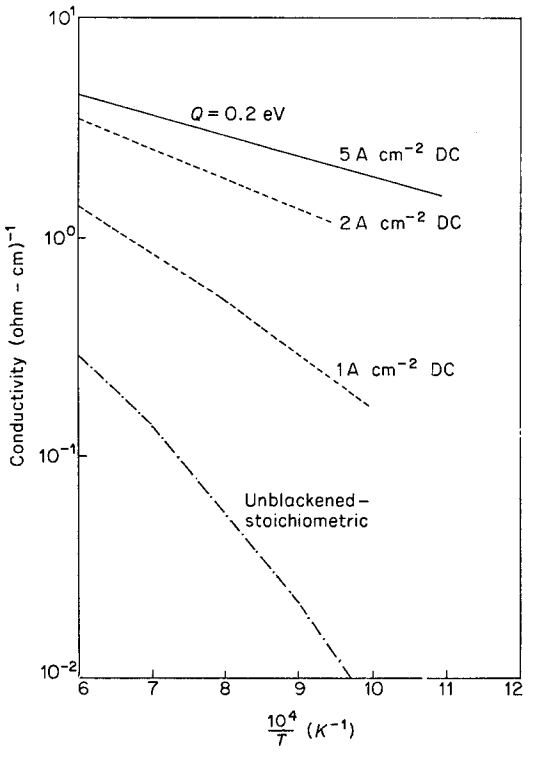

Fig. 13. Bulk conductivity of polycrystalline 12 mol % Y_2O_3:ZrO_2 blackened at 1400°C in argon, showing influence of increasing DC (blackening) current. Comparative curve for unblackened material included [13].

partial pressure on the limiting current density. The $J_L \propto P_{O_2}^{\frac{1}{4}}$ derivation applies to cells operating at low temperatures with small electrode areas [8, 9] whereas references [3] and [10] employed relatively large electrode areas at higher temperatures to arrive at a $J_L \propto P_{O_2}$ relationship. Both [3] and [10] measure $J_L \approx 10^0$ A cm^{-2} in air at 1000°C, being fully compatible with current estimates; on the other hand Yanagida [9] finds $J_L \approx 10^{-4}$ A cm^{-2} at 4×10^{-3} atm and 560°C. Extrapolation of the single crystal curve in Fig. 9 would yield a comparable value of 5×10^{-4} A cm^{-2} under the same conditions of oxygen pressure and temperature.

Yanagida [9] found the low field polarization resistance, $R_p \propto P_{O_2}^{\frac{1}{2}}$, to be mass transfer controlled ($J_L \ll J_0$), whereas the conclusion from current work at higher temperatures is that there is predominantly activation control ($J_0 < J_L$). These observations are not inconsistent when it is noted from Table 2 that the tendency for $J_L < J_0$ increases at low temperatures.

A final point of correlation comes from fitting published V–J curves to the experimental Equation 4 and extracting H/J_L and α'. Table 3 shows reasonable agreement.

4.2. *Possible mechanisms*

Table 1 gives a variety of mechanisms proposed to explain the observed rate limiting behaviour, ultimately based on either a diffusion or concentration limitation in one of the reaction species which are usually assumed to be related to the overall cathodic reduction process:

$$O_2(g) + 2V_O^{\cdot\cdot} + 4e' \rightarrow 2O_O^{\times} \qquad (7)$$

Here anion vacancies ($V_O^{\cdot\cdot}$) transported from the anode are neutralized by the reduction of gas molecules (O_2) to oxygen ions ($O_O^{\times}$) by electrons (e′) from the cathode. The potential distributions in Fig. 1 indicate an increasingly positive space charge around the cathode with decreasing ambient oxygen content. This could only arise from partial blockage of oxygen anion vacancies

Table 2. Comparison of calculated values of J_0 and experimental data for J_L for polycrystalline 12 mol % YZr as functions of P_{O_2} and T

The exchange current density J_0 was deduced from Fig. 4 using Equations A7 and A10, while the limiting current density J_L comes from the experimental Fig. 7.

	T = 1600 K		1300 K		1000 K	
	P_{O_2} = 10° (atm)	10^{-3}	10°	10^{-3}	10°	10^{-3}
J_0 (A cm^{-2})	4×10^{-2}	$1{\cdot}6 \times 10^{-4}$	8×10^{-2}	3×10^{-4}	$2{\cdot}7 \times 10^{-1}$	10^{-3}
J_L (A cm^{-2})	10°	10^{-3}	$7{\cdot}3 \times 10^{-1}$	$7{\cdot}3 \times 10^{-4}$	4×10^{-1}	4×10^{-4}

Table 3. Analysis of published V–J curves fitted to equation 4

Reference	$J_L \propto P_{O_2}$ *relation*	*Temperature* (°C)	*Oxygen partial pressure (atm)*	$\frac{H}{J_L}$	α'
Current work	$J_L \propto P_{O_2}$	1000–1400	10^{0}–10^{-3}	2	0·1→0·8 (*P&T* dependent)
[3]	$J_L \propto P_{O_2}$	1000	6×10^{-3}	0·6–1·5	0·7–0·9
[10]	$J_L \propto P_{O_2}$	1000	5×10^{-2}	0·3	0·2
Current work	$J_L \propto P_{O_2}^{\frac{1}{2}}$	<1000	10^{0}–10^{-3}	0·8	~0·1 (independent of *P&T*)
[4]	$J_L \propto P_{O_2}^{\frac{1}{2}}$	560	2×10^{-1}	0·4	0·06
[8]	$J_L \propto P_{O_2}^{\frac{1}{2}}$	800	$1{\cdot}3\times10^{-1}$	0·4–1	0·07–0·15

transported from the anode and eliminates these as a diffusion limited source. (Additionally a diffusion limited flux of anion vacancies would not lead to an observed oxygen partial pressure dependence.) Consequently the limiting mechanism must involve mass transfer of the ambient oxygen, which can approach the reaction site either by solution and diffusion through the metal electrode, by diffusion along the cathode electrode electrolyte interface or by diffusion through the electrolyte itself. The present experiment employed solid disc electrodes attached by firing at 1400°C with a fluxed platinum paste, microscopically visible as a thin layer of interfacial porous matter. Experimentally it was found that $J_L \approx 2$A cm^{-2} in pure oxygen at 1400°C. Since the diffusion limited current density is, to a first approximation, $J_L \approx (2e) D_O c_s/\delta$, where δ is the diffusion distance and c_s the surface volume concentration, using Velho and Bartlett's [17] estimates for the solubility of oxygen in platinum at 1 atm total pressure (8×10^{-5} wt %) and the corresponding atomic diffusion coefficient $D_O \approx 6\times10^{-10}$ cm^2 s^{-1}, gives a limiting current density through the Pt disc (thickness $\delta \approx 0{\cdot}2$ cm) of 4×10^{-10} A cm^{-2} at 1400°C. Furthermore, extrapolation of Simpson and Carter's [18] low temperature data for the surface exchange coefficient of oxygen in 14·2 mol % $CaO{:}ZrO_2$ to 1400°C (8×10^{-5} cm s^{-1}) and the diffusion coefficient within the same material (2×10^{-6} cm^2 s^{-1}) gives a limiting current density due to oxygen diffusion from the electrolyte surface to the interfacial reaction zone of about 4×10^{-6} A cm^{-2}. Clearly mechanisms based on oxygen diffusion through either the metal electrode or the electrolyte bulk are unable to support the measured current densities; consequently a model must assume the interfacial transport of oxygen species and requires consideration of adsorption and chemisorption of oxygen to form a cathodic interfacial double layer. An alternative mechansm which might be operative below 600°C is indicated in Section 4.5.

Although no solid platinic oxide is known to exist in the temperature range used there is evidence for a chemisorbed monolayer of (Pt-O) due to adsorption of atomic oxygen, the rate determining step being the dissociation of oxygen molecules into adsorbed atoms [19]. Both Fryburg [19] and Krier [20] propose an activation energy of 1·85 eV for the rate of oxidation of platinum within the present experimental temperature and pressure range, and it is probable that a large fraction of this energy goes into molecular dissociation. Fusy *et al.* [21] have confirmed the influence of atomic oxygen in the oxidation of platinum by observing a half-order reaction at high oxygen pressures and temperatures.

On the other hand Smith [22] has proposed that both adsorption and chemisorption occurs on pure (monoclinic) zirconia. He considered that 90–95% of the surface oxygen is irreversibly

chemisorbed in the atomic state between 500 and 1000°C, with the remaining 5–10% existing as a reversibly adsorbed mobile layer of charged O_2' molecules, the electrons contributed by anion vacancy donors. Smith considered the chemisorbed layer as a consequence of adsorbed O_2' molecules dissociating into two oxygen atoms bonded to zirconia surface sites, the activation energies for the adsorption of molecular oxygen and chemisorption of atomic oxygen being 1·5 and 2·5 eV respectively. Furthermore, Smith postulated the adsorption of oxygen molecules to be fast relative to subsequent dissociation and chemisorption as atomic oxygen; any rate limitation would consequently arise from the supply of oxygen feeding the dissociation process at a surface site, either through a flux limit in the ambient gas or its diffusion to the reaction site.

It is suggested that these concepts may also apply to the diffusion of oxygen along the interface between a solid impermeable metal electrode and a stabilized zirconia electrolyte, such that the overall reaction proceeds as:

adsorption of O_2 gas at the gas-interface annulus followed by diffusion along interface to the reaction site, then chemisorption at reaction site and finally the reduction reaction. (8)

4.3. *The low field rate determining step*

It was shown in Section 3.2.1. that the polarization resistance is relatively uninfluenced by mass transfer, and the exchange current density for the activated reaction 7 determined as

$$J_0 = 2{\cdot}9 \times 10^{-18} c_g^{0.8} \exp(0{\cdot}315\beta) \qquad (9)$$

The problem is to consider the possible intermediates of reaction 7, uninfluenced by mass transfer steps which will satisfy the experimental Equation 9. Suppose reaction 7 occurs along the following steps:

$$O_2 \rightarrow 2O(\text{adsorbed site}) \qquad (7a)$$

$$\left.\begin{array}{l} 2[O + e' \rightarrow O'] \\ 2[O' + e' \rightarrow O''] \\ 2[O'' + V_O^{\cdot\cdot} \rightarrow O_O^{\times}] \end{array}\right\} \text{(chemisorbed site)} \quad \begin{array}{l} (7b) \\ (7c) \\ (7d) \end{array}$$

If 7a is the rate determining step (r.d.s.) then the exchange current density $J_0 \propto c_g$ and independent of the symmetry factor for an electronation step [23]. On the other hand the reversible e.m.f. of a galvanic cell based on stabilized zirconia requires that the ratio of the total number of electrons transferred in the overall reaction to the stoichiometric number, $n/\nu = 4$, in the Nernst equation, or ν to equal unity. This eliminates any of steps 7(b–d) as the r.d.s., which would, in any case, push step 7a into quasi-equilibrium and lead to $J_0 \approx c_g^{(\frac{1}{2} - f\alpha)}$ (where f is some fraction), which is inconsistent with an experimental exponent of 0·8.

As a model based on complete electron transfer at the chemisorbed site is incompatible with experiment, it is necessary to examine the merits of a charged mobile adsorbed species. Let the intermediates of reaction 7 be:

$$O_2 + e' \rightarrow O_2' \quad \text{(adsorbed site)} \qquad (7a')$$

$$\left.\begin{array}{l} O_2' + e' \rightarrow 2O' \\ 2[O' + e' \rightarrow O''] \end{array}\right\} \begin{array}{l} \text{(either adsorbed or} \\ \text{chemisorbed site)} \end{array} \quad \begin{array}{l} (7b') \\ (7c') \end{array}$$

$$2[O'' + V_O^{\cdot\cdot} \rightarrow O_O^{\times}] \quad \text{(chemisorbed site)} \qquad (7d')$$

As before, either Equation 7c′ or 7d′ as the r.d.s. will lead to an exponent of $c_g < \frac{1}{2}$. Appendix A considers the exchange current densities resulting from either of steps 7a′ and 7b′ as r.d.s. which lead respectively to $J_0 \propto c_g^{1-\alpha/4}$ or $J_0 \propto c^{1-(1+\alpha/4)}$.

The magnitude of the symmetry factor governing the rate determining, charge transfer step will control the exponent n in the $J_0 \propto c_g^n$ relation. The respective limits on n for reactions 7a′ and 7b′ as r.d.s. are $0{\cdot}75 < n < 1$ and $\frac{1}{2} < n < 3/4$ as $1 > \alpha > 0$. The experimental data are not accurate enough to insist that the exponent $n = 0{\cdot}8_0$ lies outside the limits required by step 7b′ as the r.d.s., and the choice between the two possible r.d.s. must be made by considering the relative magnitude of α. If step 7a′ is the r.d.s., then $\alpha = 0{\cdot}8$ to give $n = 0{\cdot}8$, whereas $\alpha \rightarrow 0$ for 7b′ as the rate determining step. The latter condition is tantamount to reaction 7b′ being rapid in the forward direction and strongly retarded in the reverse, contrary to the requirement of a cathodic r.d.s. Consequently, step 7a′ is considered to be the r.d.s. for the overall cathodic reaction 7, and would correspond to Smith's model [22] if it were contended that steps 7b′–d′ in tandem occurred at a chemisorption site following mobile adsorption of O_2'. This is consistent with

ESR experiments on related oxides [24, 25] which detected adsorbed O_2^- on exposed surfaces, but the knowledge that at high temperatures the platinic surface oxide involves the atomic species does yield the possibility that chemisorption of atomic oxygen occurs on both the electrode and electrolyte interface surfaces.

4.4. *The approach to the rate limit*

It was demonstrated in Section 3.2.2. that the simple Nernst diffusion model fails to relate to the experimental results which are, however, satisfied by the more complex Equation 4.

The basis of the theoretical model developed in Appendix B to arrive at the experimental Equation 4 is the solution of the steady state continuity equation for the sequential reaction 8 which is subject to two fundamental postulates. Firstly the adsorption of oxygen gas molecules in the vicinity of the annular gas-interface boundary (the triple contact boundary between the metal electrode, electrolyte and gas phase) can be represented by a simple surface exchange mechanism, described mathematically by continuity of the concentration gradient over, and just within, the annular plane (Equation B1). Secondly, the chemisorption of a mobile interfacial oxygen species onto the electrolyte surface and its consequential reaction with an anion vacancy (which may be associated with a chemisorbed atom as a bound complex) is likely to be fast relative to the mass transfer step, and may be described by the modified Butler–Volmer Equation B2.

Solving the continuity equation subject to these postulates leads to the experimental Equation 4, and shows that the constant factor H depends on the magnitude of the forward part of the reaction current density in Equation B2. As expected for the case of strong activation, H reduces to the partial reaction exchange current density, but it is more likely that the approach to the mass transfer limit, as in the current experiment, pushes H into a more complex relation as given in Equation B11b.

The theory presented in Appendix B, primarily to justify the necessity of assuming a surface exchange mechanism, makes no specific demands on the nature of the interfacial charge transfer mechanism; any attempt to correlate α_r' of Appendix B with the equilibrium symmetry coefficient α in Appendix A is unjustified. Furthermore, it was emphasized in Equation 5 that α_r' is modulated by the concentration overpotential; Fig. 10 illustrates that this factor is very significant in the polycrystalline material for which a flux limiting mechanism is considered to operate. Accordingly any further evaluation of the pre-exponential factor (H/J_L) from the theoretical Equation B11 is inappropriate other than to demonstrate that a rough estimate shows J_{0r} to be large compared to J_0, as it must be for J_0 to represent the low field r.d.s.: since

$$\left(\frac{H}{J_L}\right)^2 \approx 1 = \frac{J_{0r}}{2eh\bar{c}_O}\cdot\frac{D}{\gamma^2},$$

with $\dfrac{D}{\gamma^2}\sim\left(\dfrac{kT}{h^*\lambda}\right)^2\Big/\left(\dfrac{kT}{h^*\lambda}\right)^2 \approx 10^{-14}$, $\bar{c}_O \approx 10^{19}$ cm^{-3}, $h\approx 10^{-4}$ cm gives $J_{0r}\approx 10^4$ A cm^{-2}.

4.5. *The high field rate limiting steps*

The sequence of the low field electrochemical steps is often destroyed by the imposition of a mass transfer rate limit, since activation processes are governed by the rate of charge transfer and become difficult when the adsorbed layer is depleted [26]. Consequently knowledge of the reaction sequence 7a′–7d′ fails to provide any direct information on the nature of the rate limiting mechanism.

Reference to Fig. 14 depicting the progressive steps across the gas-interface annulus shows that under low field equilibrium detailed balance gives

$$\sigma f\Gamma_g = \Gamma_a(=\gamma(c_O - c_R)) = \Gamma_i,$$

where the Γ's are fluxes, σ the gaseous condensation coefficient and f the probability of an exposed adsorption site. Consideration leads to the conclusion that three possible limiting conditions exist:

(a) Gas flux limit, for which the adsorption probability $f\to 1$ and the limiting current density $J_L = 4e\sigma\Gamma_g \propto P_{O_2}$.
(b) Diffusion flux limit, under which condition the limiting interfacial flux Γ_{iL} raises the

annular concentration c_R to a limiting value c_{RL} in relation to a detailed balance between the surface exchange and diffusion coefficients; accordingly $J_L = 2e\gamma(c_O - c_{RL}) \propto (P_{O_2}^{\frac{1}{2}} - C)$ if molecular dissociation of oxygen precedes surface exchange.

(c) Surface exchange flux limit, for which the adsorption flux approaches a limiting value $\Gamma_{aL} = \gamma c_O \propto P_{O_2}^{\frac{1}{2}}$ if a preceding dissociative step is forced into equilibrium.

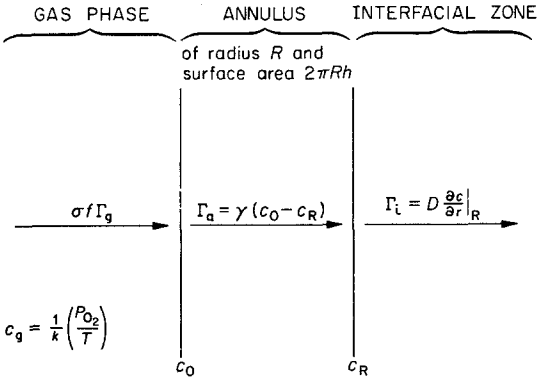

Fig. 14. Sketch showing balance of fluxes on surface exchange at the gas-interface annulus.

Γ's are fluxes.

γ, D are respectively the surface exchange and diffusion coefficients.

σ, f are the condensation and adsorption probability of the oxygen molecule at the annulus.

It has been demonstrated that $J_L \propto P_{O_2}$ in polycrystalline 12 mol % YZr, which is attributed to limiting mass transfer of the ambient gas flux Γ_g. Considering the situation where the gas flux condenses on an annulus of area $2\pi Rh$, the limiting condensation rate is $2\pi Rh\sigma\Gamma_g$, where the condensation coefficient σ involves an enthalpy of condensation ΔH_c: $\sigma = \sigma_0 \exp(-\Delta H_c/kT)$ and $\Gamma_g = P_{O_2}(2\pi mkT)^{-\frac{1}{2}}$ from kinetic theory. Assuming a uniform flux of vacancies Γ_V across the electrolyte, and equating the vacancy current to the condensation current gives $\pi R^2 \Gamma_V(2e) = 2\pi Rh\sigma\Gamma_g(4e)$ and

$$J_L = 2e\Gamma_V = \frac{8he\sigma_0}{(2\pi mk)^{\frac{1}{2}}R}\left(\frac{P_{O_2}}{T^{\frac{1}{2}}}\right)\exp-\frac{\Delta H_c}{kT} \quad (10)$$

which is the experimental Equation 6. The condensation enthalpy $\Delta H_c = 0{\cdot}26$ eV compares with 0·32 eV evaluated by analysis of Fig. 7 of reference [3], and as reasonably expected is of the order of the enthalpy of van der Waal forces. Experimentally, the constant $8he\sigma_0/(2\pi mk)^{\frac{1}{2}}R = 275$ (P_{O_2} in atm) and suggests that $h\sigma_O \approx 10^{-5}$ cm s^{-1}. Taking h as the thickness of the interface, estimated optically as a few micrometres, shows that a reasonable value of σ_O is 10^{-1}.

The experimental data for the single crystal 8·3 mol % YZr exhibits a flux limit at high temperatures, but tends towards another mechanism below about 800°C. Unfortunately current results do not permit an unequivocal analysis of the low temperature data, other than to indicate a tendency to $J_L \propto P_{O_2}^{\frac{1}{2}}$ with an activation energy of 1 eV in agreement with both Kleitz [8] and Yanagida [9]. More explicitly, both these authors have directly measured a potential independent $J_L \propto P_{O_2}^{\frac{1}{2}}$ characteristic without the constant factor $C = c_{RL}$ required for the diffusion limit, case (b) above. It is easily seen that for the diffusion limit

$$\gamma(c_O - c_{RL}) = D\left|\frac{\partial c}{\partial r}\right|_R \approx \frac{Dc_{RL}}{\delta},$$

whereas for surface exchange limit $c_{RL} \to 0$ and γc_O must be much greater than the limiting diffusion flux, i.e. $\gamma c_O \gg Dc_{RL}/\delta$ (δ is an effective diffusion length). On the basis of simple microscopic flow theory the surface exchange coefficient is of the order of the product of the atomic vibration frequency and atomic jump distance, $\gamma \approx kT/h^* \times \lambda$, where h^* is Planck's constant; and also $D \approx kT/h^* \times \lambda^2$ and $\gamma/D \approx \lambda^{-1}$. Provided that $\delta \gg \lambda$ then $(c_O - c_{RL}) \to 0$, contrary to observation. This simple argument would suggest that the low-temperature rate-limiting mechanism arises from the coupling of molecular dissociation and surface exchange in preference to interfacial diffusion.

The tenuousness of this argument does not invalidate the derivation of the limiting current density; consider the molecular dissociation of oxygen into an activated complex as being in quasi-equilibrium at the gas-interface annulus:

$$O_2(g) + S\ (\text{site}) \rightleftharpoons 2O$$

for which mass action provides $K_a = c_O^2/c_g N_S$; N_S being the surface concentration of active sites at the annulus. The rate of transfer of the activated complex over a potential energy

barrier (E_a) onto the mobile interfacial layer is

$$v = \frac{kT}{h^*}\lambda c_O \exp\left(-\frac{E_a}{kT}\right),$$

where λ is of the order of atomic dimensions. Writing the equilibrium constant $K_a = \exp(\Delta S_a/k)\exp(-\Delta H_a/kT)$, with ΔS_a, ΔH_a the entropy and enthalpy respectively for molecular dissociation, then as before the limiting current density

$$J_L = 2e\Gamma_V = \frac{2\pi Rhv(2e)}{\pi R^2}$$

$$= \frac{4he}{R}\cdot\frac{kT}{h^*}\cdot\lambda(N_S c_g)^{\frac{1}{2}}\exp\left(\frac{\Delta S_a}{2k}\right)\exp-\left(\frac{E_a+\Delta H_a/2}{kT}\right)$$

$$= A_0\left(\frac{P_{O_2}}{T}\right)^{\frac{1}{2}}\exp-\frac{Q}{kT} \qquad (11)$$

$$A_0 = \frac{4hekT\lambda}{h^*R}\left(N_S\frac{10^{22}}{1{\cdot}38}\right)^{\frac{1}{2}}\exp\left(\frac{\Delta S_a}{2k}\right)\approx 5\times 10^5;$$

$$Q = \left(E_a+\frac{\Delta H_a}{2}\right)\approx 1\ \text{eV}$$

experimentally from Fig. 9. (Although A_0 strictly includes a temperature factor the expression has been retained in this form to conform to the trend shown in Fig. 9.) Both Fryburg [19] and Krier [20] quote an activation energy of 1·85 eV for surface oxidation of Pt around 1000°C and the current estimate for Q is compatible if this is compared to ΔH_a, and E_a to the enthalpy for van der Waals forces. The experimental estimates for A_0, with $h\approx 10^{-4}$ cm, $T\approx 1000$ K and $\lambda\approx 3\times 10^{-8}$ cm requires that $N_S^{\frac{1}{2}}\exp(\Delta S_a/2k)\approx 5\times 10^{10}$ cm^{-1}; putting $N_S\approx 10^{14}$ cm^{-2} as a typical surface concentration of activation sites gives $\Delta S_a\approx 1{\cdot}45\times 10^{-3}$ eV K^{-1} ($\equiv 33$ cal mol^{-1}K^{-1}). To a first approximation, ΔS_a may be compared to the difference in entropy between atomic and molecular oxygen, $\Delta S_a = (2S_O - S_{O_2}) = 31$ cal mol^{-1} K^{-1} at 1000 K, using the tabulated data in reference [28].

No clear picture of the adsorption mechanism is possible, but the correspondence in activation energies suggests that molecular dissociation of oxygen is localized on the metal electrode surface in the vicinity of the triple contact annulus before transfer to the mobile interfacial layer. Some support for this hypothesis follows from Kleitz's [8] observation that the metal electrode influences the limiting current density such that J_L decreases in the order Ag–Pt 10% Rh–Rh, corresponding to decreasing oxidation potentials.

Reference to Fig. 9 shows that a low temperature $J_L \propto P_{O_2}^{\frac{1}{4}}$ regime was not observed in polycrystalline 12 mol % YZr, but it would not be unreasonable to expect its existence at lower temperatures, below 800°C. Comparison with earlier workers, particularly Etsell [3], Brook [4] and Kleitz [8] reveals that choice of experimental conditions controls the detailed balance between the flux limiting and adsorption limiting mechanisms. Kleitz deduced a $J_L \propto P_{O_2}^{\frac{1}{2}}$ behaviour between 750 and 1200°C using a point electrode; this would be compatible with the proposed model if the capture area corresponded to the gas-interface annulus, without adsorption on the exposed metal or electrolyte surface, followed by mobile transfer to the annulus. On the other hand the distinction in the conclusions arrived at by Etsell [3] and Yanagida [9], who both used fired Pt paste electrodes, is that the latter-deduced a $J_L \propto P_{O_2}^{\frac{1}{2}}$ relation using small electrodes (<1mm^2) at 560°C whereas Etsell concluded that large area electrodes ($\approx$100mm^2) gave a direct $J_L \propto P_{O_2}$ proportionality between 700 and 1100°C. Conversely Brook [4] has presented evidence that a flux in the Pt paste exerts a controlling influence in acting as a sealant to pores in incompletely fired Pt paste, thereby preventing direct access of oxygen to the interface and minimizing the effective triple contact boundary area. Similarly Karpachev [29] increased the triple contact boundary area by scratching lines on the fired Pt paste electrode and observed a corresponding increase in the limiting current density.

However, Brook [4] demonstrated that the limiting current density in 15 mol % CaO:ZrO$_2$ at 520°C was inversely proportional to the thickness of Pt foil electrodes, between 30 and 120 μm thick, which strongly suggests that the limiting mechanism involves oxygen diffusion through the foil. Current work in the author's laboratory has indicated that the Seebeck coefficient of 12 mol % YZr in contact with Pt disc electrodes falls to zero below about 500°C. Current work using other metal electrodes with

YZr may explain the influence of the metal in controlling the interfacial phenomena. This could indicate that the mobility of the interfacial species may be too low to sustain the heterogeneous (electrode reaction) contribution to the total thermoelectric power, thereby allowing a second mechanism, based on oxygen diffusion through the electrode, to dominate. Nevertheless, Brook *et al.* [4] and Kroger [46] were unable to correlate their mass transfer data with oxygen diffusion and solubility data in platinum.

Summarizing, it would appear justified to postulate that above about 500–600°C the limiting current density J_L which may be sustained prior to blackening is insensitive to the cathode structure (paste, foil or solid disc). Instead, it is considered that temperature and electrode configuration, through the effective area of the triple contact boundary, are the controlling factors. Only in this way is it possible to correlate existing experimental data, such that at low temperature and small electrode radius, molecular dissociation of oxygen dominates; whereas at high temperature and large effective capture area the oxygen condensation flux is rate controlling. Consequently Karpachev's [29] observation that J_L could be magnified by increasing the effective capture length with lines scoured through the electrode can be accommodated. Conversely J_L would decrease if the effective height (h) of the triple contact boundary were diminished through the use of a flux as the sealant [4].

Practical systems utilizing stabilized zirconia as power devices, such as open cycle MHD electrodes or fuel cells, require operation in a regime of the V–J curve exhibiting minimum polarization loss and freedom from destruction by blackening. Examination of Fig. 2a reveals that atmospherically this condition will only be met in pure oxygen (or possibly CO_2) when operating near the point X at which blackening commences. Commensurate with this requirement is the need to maximize J_L, and to this end the model raised above proposes that this will be achieved by use of an electrode configuration having a large triple contact boundary area. Qualitative results using a laboratory scale-seeded MHD burner did suggest that a stabilized zirconia electrolyte contacted to a Pt disc cathode having a number of drilled holes was less susceptible to blackening; however the reduced surface area of contact led to a weaker electrode-electrolyte bond [14].

4.6. *Blackening in yttria stabilized zirconia*

Turning now to the problem of initiation of blackening it would be reasonable to anticipate that the mass transfer limit leads to an effectively blocking cathode with interfacial depletion of adsorbed oxygen. Consequently the polarization field would lower the potential barrier between the electrode and electrolyte sufficiently to permit thermionic emission of electrons across the interface with subsequent trapping in accumulated anion vacancies. The F centres so created would lead to the observed space charge region in Fig. 1c.

The equivalent electrical circuit for the electrode polarization in an ionic conductor is a parallel combination of equivalent capacity and resistance, representing respectively the non-discharge of vacancies at the blocking electrode and the effective polarization of the electrode reaction [31]. When the concentration overpotential η_c reaches a limiting value η_L, the charge accumulation on the equivalent capacitor permits field lowering of the electrode-electrolyte barrier of height ϕ_0; the Richardson–Schottky equation applies for thermionic emission across a potential step with attendant image forces [32]:

$$J = 120T^2 \exp - \left[\frac{\phi_0 - \left(\frac{(2e)^3 \eta_L}{4\pi\varepsilon^* \varepsilon_0 L} \right)^{\frac{1}{2}}}{kT} \right]$$

where η_L/L is the polarization field across the equivalent capacitor of width L equal to the Debye length [33] and ε^* the high frequency dielectric constant. Fig. 15 shows the application of this equation to the envelope of curves such as A–B in Fig. 12, (using η_L from Fig. 11 in place of the total voltage V); $\phi_0 = 5{\cdot}4$ eV and $\varepsilon^* L = 2 \times 10^{-7}$. Assuming ε^* of the order of 5–10 (the static value is about 40 for 8·3 mol % YZr [34]) gives $L \approx 2{\cdot}5 \times 10^{-8}$ cm, being twice the diameter of an oxygen atom [35]. The equivalent electrode capacitance may be calculated as $C = \varepsilon\varepsilon_0/L \approx 140\,\mu\text{F cm}^{-2}$ (ε now the static dielectric constant,

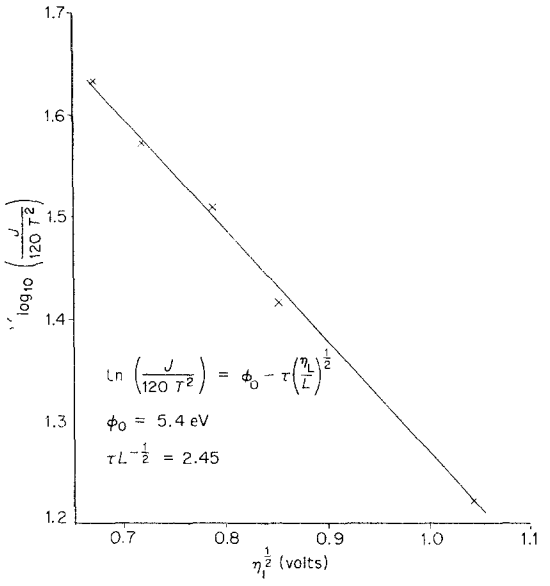

Fig. 15. Plot of $\log_{10}(J/120T^2)$ versus $\eta_L^{\frac{1}{2}}$ for the thermionic emission region of Fig. 12, for $T = 1380$°C.

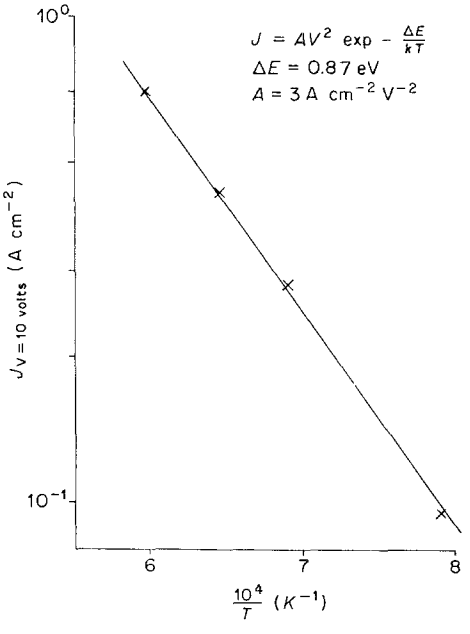

Fig. 16. Plot of Equation 12 showing the influence of trap levels on the space charge limited conduction of regime Fig. 12. The current density J is taken for $V = 10$V.

40) which is in good agreement with direct measurements by Bauerle [6] made under low field AC conditions. Bauerle found the capacitance was relatively insensitive to oxygen partial pressure and electrode configuration; the present correspondence suggests that the dominant influence could be chemisorbed oxygen atoms on one or both surfaces of the interfacial components, and refers back to Smiths' postulate [22] that only 5% of the available oxygen is reversibly adsorbed on free zirconia. The areal space charge density on the equivalent condenser (N) follows since $C = N(2e)/\eta_L$, giving $N \approx 3 \times 10^{14}$ cm^{-2} at $\eta_L = 0{\cdot}8$ V. Since the surface density of anion vacancies fixed at 5% occupancy by the yttria dopant concentration is 7×10^{13} cm^{-2}, this would indicate that some vacancy accumulation may occur at the cathode prior to electron injection.

4.6.1. *Quadratic V–J characteristic.* It is significant that the electronic part of the cathodic V–J characteristics tends to a $J \propto V^2$ relation accurate over at least a decade. There is little or no ionic polarization in this regime (Fig. 1c) and the voltage drop due to bulk resistive effects in the sample between the electrode and probe is much less than 0·1 V, so that the $J \propto V^2$ regime must represent an interfacial phenomenon. The quadratic characteristic is exhibited equally by a 'well-blackened' sample in argon and by a sample in oxygen which is known to exhibit just an initial discolouration around the cathode under these conditions.

Extrapolation of the linear $J_L \propto P_{O_2}$ relation obtained for the diffusion limit between 10^{-3} and 10^{-1} atm oxygen did not agree with the estimated diffusion limited current density for pure oxygen. Instead, blackening occurred at lower current densities, approximately where the pure oxygen ohmic $J \propto V$ curve intersected the quadratic $J \propto V^2$ curve (point X on Fig. 2a), however the evidence is based entirely on visual observation of cathodic discolouration. Similar quadratic characteristics were noticed above 1 V in the single crystal material and also in an isolated polycrystalline sample of 17 mol % $MgO:ZrO_2$. Cardon [36] has reported a $J \approx V^2$ characteristic in thin slices of rutile (TiO_2) which was attributed to space charge limited current at the positive electrode. However, it is clear that the phenomenon in YZr is localized at the cathode interface and exhibits a strong temperature effect (B–C of Fig. 12).

The theory of space charge limited (SCL) conduction in the presence of electron traps has been adequately covered elsewhere [37–39]. The space charge limited current is:

$$J_{SCL} = \frac{9}{8} \cdot \frac{\varepsilon\varepsilon_0\mu_0\theta V^2}{8d^3} \qquad (12)$$

where μ_0 is the microscopic electron mobility, d the width of the space charge region and θ the ratio of free to trapped charge given by [38], $\theta = (N_s/N_t).\exp-(\Delta E/kT)$, N_s is the density of states at the bottom of the conduction band, being of the order of the concentration of atoms in zirconia (10^{23} cm^{-3}) and N_t the density of traps positioned an energy ΔE below the conduction band. Lampert [39] has shown that the transition from ohmic to SCL conduction occurs at a voltage:

$$V_{SCL} = \frac{(2e)\ N_0 d^2}{\theta\varepsilon\varepsilon_0} \qquad (13)$$

as does indeed occur at about 5V in YZr for pure oxygen at the highest temperatures, where little polarization is present (point X of Fig. 2a). N_0 is the density of free electrons in the electrolyte, related to N_s through the band gap E_g by $N_0 = N_s \exp-(E_g/2kT)$.

A plot of log J versus $1/T$ in Fig. 16 for V = 10 V from Fig. 12 gives a straight line of slope $\Delta E = 0{\cdot}87$ eV and intercept $\frac{9}{8}\frac{\varepsilon\varepsilon_0\mu_0}{d^3}\frac{N_S}{N_t} =$ 3A cm^{2}V^{-2}. If the density of traps is taken to be the concentration of anion vacancies fixed by composition at 3×10^{21} cm^{-3} and the electron mobility as 0·1 cm^2(Vs)$^{-1}$ (Section 4.6.2. below), then the width of the space charge limited region is calculated to be $d\approx3{\cdot}5\times10^{-3}$ cm. Substituting back in Equation 13 with V_{SCL} = 5 V yields a band gap $E_g\approx3{\cdot}4$ eV for YZr at 1500 K which may be compared to room temperature optical absorption estimates of 3·8 eV [40].

It is not possible to do more than speculate on the nature of the electrode space charge limited region of about 35 μm width, having trap levels 0·87 eV below the conduction band. There is some evidence [41] to suggest that trap levels at 0·8 eV could be associated with chemisorbed O′ surface states; on the other hand the consequential diffusion of Pt on blackening leads to the formation of an intermetallic Pt(Y,Zr) phase just within the electrolyte [42] and it may be significant that the estimated depth of the space charge region approaches that of the visually observed depth of penetration of Pt into the electrolyte (100 μm).

4.6.2. *High field electronic conduction in yttria stabilized zirconia.* The stabilization of the lnσ–1/T curve in Fig. 13 for the electronic conduction mode in the blackened material represents a saturation state within the bulk electrolyte independently of electrode limited space charge processes. Jacquin [2] has shown that conduction in the blackened state tends to an exclusively electronic contribution, and whilst it is impossible to define a state of 'saturation blackening', it does not seem unreasonable that the reproducible state is associated with a completely electronic conductor. An activation energy of 0·2 eV is typical for electron hopping between anion vacancy acceptors and a rough estimate of the mobility at 1000°C may be estimated by taking the electronic conductivity to be 3 (ohm cm)$^{-1}$, and assuming electrons to be completely trapped by the available vacancies (whose concentration is fixed by the degree of aliovalent stabilization) a mobility of the order of 0·1 cm^2 (V s)$^{-1}$ is estimated. Whilst the assumption of complete trapping is probably unjustified, giving too low a mobility, it does approach the typically expected mobility values for electron hopping. The crucial test for electron hopping is the existence of a direct Boltzmann type relation for the mobility, for which evidence is at present lacking.

4.6.3. *The nature of blackening.* Finally a few comments are offered on the nature of blackening in stabilized zirconia which does not appear to have been adequately considered elsewhere. The current work has demonstrated that blackening is a direct consequence of electron injection from the metal electrode into anion vacancies accumulated at the blocking cathode to give a 'saturated' electronic conduction mode. The potential distribution in Fig. 1c and evaluation of photographs of quenched specimens (see reference [15] for photographic details) reveal that the progressive movement of the blackened

zone is governed by temperature, current density and oxygen partial pressure. Furthermore, the geometry of the interface between the blackened and stoichiometric zones is a tongued-shaped configuration in cylindrical specimens. It is believed that the final position of the tongue-shaped blackened zone is a true equilibrium, represented by a balance between hopping of electrons through the blackened zone, oxygen diffusion from the cylindrical sides of the sample, and mass transport of anion vacancies from the anode. In other words the interface between black and white zirconia behaves as a 'virtual cathode'.

The trapping of injected electrons into vacancies, which may or may not be associated, would be expected to manifest itself both in ESR measurements and through optical absorption by colour centres. Thorp [43] consequent to blackening, has found ESR evidence for an isotropic F centre, consisting of an oxygen anion vacancy with a trapped electron and surrounded by a cationic tetrahedral configuration of zirconium ions. On the other hand the band edge for single crystal 8·3 mol % YZr has been found to shift from 2750 Å to around 1 μm on blackening [30, 40]. Qualitatively therefore, blackening corresponds to complete absorption over the visible spectrum, but the fundamental mechanism is as yet far from clear. The existence of a well-defined F centre would be expected to manifest itself as a small but prominent peak in the absorption curve somewhere between the band edge and phonon absorption edge at 10 μm; this has never been observed. Wright *et al.* [30] have shown that blackening is accompanied by strong scattering over the entire visible spectrum due to colloidal particles in the 100–500 Å diameter range; the shift in apparent band edge on blackening corresponding to the long wavelength edge of the colloidal scattering spectrum. Wright *et al.* believe the colloids to be zirconium metal particles precipitated as a consequence of anion vacancy aggregation, although direct detection of such metallic precipitate has never been achieved. This should not be confused with the semi-metallic zirconium oxynitride formed on blackening in a nitrogen-rich environment [44]. It is interesting to speculate on their relation to the 'syntatic zones' observed by Carter and Roth [45] which were said to be made up of ordered clusters of complexes up to 600 Å diameter. These were observed by electron microscopy of stoichiometric CaZr single crystals, and it is an arguable point whether stoichiometry was retained during electron bombardment. If this were not so, electron trapping within such syntactic zones may cause clusters of colour centres with a broad absorption band over the entire visible spectrum, having conduction by a thermally assisted hopping mechanism.

5. Conclusions and summary

It has been demonstrated that while differences arise in interpretation, all existing work on the rate-limiting mechanism in stabilized zirconia are experimentally consistent within the limitations of the adopted experimental conditions.

Summarizing the sequence of the conduction modes and V–J characteristic, it has been well established that at low fields the conduction is entirely ionic, due to oxygen anion vacancy transport; there is evidence to suggest that only a small fraction of vacancies are free to conduct, owing to association with cationic defects [13]. Both cathodic and anodic electrode reactions, represented overall by Equation 7 and its converse, exhibit ohmic characteristics for current densities well below J_0 which itself is a function of ambient oxygen partial pressure and temperature (Table 2). Consequently the low field ohmic resistance is activation controlled above 800°C but there is some evidence to show a mass transfer influence at lower temperatures [9]. The rate determining step in the cathodic reaction 7 is considered to be the electronation of an oxygen molecule in the vicinity of the gas-interface annulus. This O_2' species is believed to be adsorbed onto the interface; further dissociation and electronation then takes place to replenish a chemisorbed site which may itself be associated with an underlying oxygen anion vacancy prior to neutralization, according to Equation 7d′.

The expected transition to a Tafel behaviour has not been observed in this and other work owing to the masking influence of mass transfer associated with the gas phase. The nature of the rate-limiting mechanism depends on experiment,

particularly temperature and diameter of electrode. At high temperatures and large triple contact boundary annular areas, the ambient gas flux striking the exposed annulus is rate limiting, whereas point electrodes or low temperatures lead to molecular dissociation followed by surface exchange into the interface as the controlling factor.

Because of the rate-limiting mechanism there is an accumulation of anion vacancies at the (effectively) blocking cathode with field lowering of the interfacial potential barrier to permit thermionic emission of electrons which are trapped in oxygen anion vacancies. Subsequent to blackening, even at quite low current densities, an intermetallic Pt(Y,Zr) phase forms in the electrolyte adjacent to the interface which may control the space charge limited conduction at the cathode. However, the bulk conduction becomes saturated at high bias fields, the activation energy for the ensuing electronic conduction being about 0·2 eV compared to 0·7–0·9 eV for the stoichiometric material. This and the calculated mobility, favour hopping of electrons trapped in uncompensated anionic vacancies as the dominant conduction process.

Appendix A

Derivation of the exchange current density for the overall reaction 7

Consider the intermediates of reaction 7 proposed in Section 4.2:

$$O_2 + e' \rightarrow O_2' \quad (7a')$$
$$O_2' + e' \rightarrow 2O' \quad (7b')$$
$$2[O' + e' \rightarrow O''] \quad (7c')$$
$$2[O'' + V_O^{\cdot\cdot} \rightarrow O_O^{\times}] \quad (7d')$$

for which the charge transfer r.d.s. may be either 7a′ or 7b′.

Considering step 7a′ as the r.d.s., the partial current density is

$$j_a = ek_a'[O_2]\exp(-\alpha\beta\Delta\phi) - ek_a''[O_2']\exp(1-\alpha)\beta\Delta\phi \quad (A1)$$

where $\beta = (kT)^{-1}$, α the symmetry factor, $\Delta\phi$ the non-equilibrium potential supporting the charge transfer and k_a', k_a'' the forward and reverse rate constants respectively. Since all succeeding steps are in quasi-equilibrium:

$$k_b'[O_2']\exp-\alpha\beta\Delta\phi = k_b''[O']^2\exp(1-\alpha)\beta\Delta\phi$$
$$k_c'[O']\exp-\alpha\beta\Delta\phi = k_c''[O'']\exp(1-\alpha)\beta\Delta\phi$$
$$k_d'[O''][V_O^{\cdot\cdot}] = k_d''[O_O^{\times}]$$

The partial current density for the r.d.s. 7a′ becomes

$$j_a = ek_a'c_g\exp(-\alpha\beta\Delta\phi) - ek_a''\cdot\frac{k_b''}{k_b'}\left(\frac{k_c''k_d''}{k_c'k_d'}\right)^2\frac{[O_O^{\times}]^2}{[V_O^{\cdot\cdot}]^2}\cdot\exp(4-\alpha)\beta\Delta\phi$$

$$= eK_a'c_g\exp(-\alpha\beta\Delta\phi) - eK_a''\frac{[O_O^{\times}]^2}{[V_O^{\cdot\cdot}]^2}\cdot\exp(4-\alpha)\beta\Delta\phi$$

By definition, the partial exchange current density at equilibrium ($j_a = 0$, $\Delta\phi = \Delta\phi_0$) is:

$$j_{0a} = eK_a'c_g\exp-\alpha\beta\Delta\phi_0 = eK_a''\frac{[O_O^{\times}]^2}{[V_O^{\cdot\cdot}]^2}\exp(4-\alpha)\beta\Delta\phi_0 \quad (A2)$$

$$\text{or } \Delta\phi_0 = \frac{1}{4\beta}\cdot\ln\frac{K_a'}{K_a''}c_g\frac{[V_O^{\cdot\cdot}]^2}{[O_O^{\times}]^2} = \varepsilon_0 + \frac{1}{4\beta}\ln c_g\frac{[V_O^{\cdot\cdot}]^2}{[O_O^{\times}]^2} \quad (A3)$$

which on substituting back into Equation A2 yields:

$$j_{0a} = eK_a'\left(\frac{[O_O^{\times}]}{[V_O^{\cdot\cdot}]}\right)^{\alpha/2}\cdot c_g^{(1-\alpha/4)}\exp-\alpha\beta\varepsilon_0 \quad (A4)$$

$\varepsilon_0 = 1/4\beta\,.\ln K_a'/K_a''$, is the reversible potential for the partial reaction. The overall exchange current density for the complete reaction 7 assuming step 7a′ as the r.d.s. is:

$$J_0 = 4j_{0a} = \bar{K}_a c_g^{(1-\alpha/4)}\exp-\alpha\beta\varepsilon_0 \quad (A5)$$

since $[O_O^{\times}]$ and $[V_O^{\cdot\cdot}]$ are constants fixed by the electrolyte concentration.

The remaining possibility is to consider step 7b′ as rate determining. Proceeding as before, the partial current density is:

$$j_b = ek'_b[O'_2]\exp(-\alpha\beta\Delta\phi) - ek''_b[O']^2\exp(1-\alpha)\beta\Delta\phi$$
$$= eK'_b c_g \exp\{-(1+\alpha)\beta\Delta\phi\} - eK''_b \frac{[O_O^\times]^2}{[V_O^{\cdot\cdot}]^2}\exp(3-\alpha)\beta\Delta\phi$$

At equilibrium, $j_b = 0$, $\Delta\phi = \Delta\phi_0$ and the overall exchange current density:

$$J_0 = 4j_{0b} = 4eK'_b\left(\frac{[O_O^\times]}{[V_O^{\cdot\cdot}]}\right)^{\frac{1+\alpha}{2}} c_g^{\left(\frac{1-1+\alpha}{4}\right)} \times \exp-(1+\alpha)\beta\varepsilon_0$$
$$= \bar{K}_b c_g^{\left(\frac{1-1+\alpha}{4}\right)}\exp-(1-\alpha)\beta\varepsilon_0 \qquad (A6)$$

The rate constant $k_i = k_{i0}\exp-(\beta\Delta G_0^\#)$, where $\Delta G_0^\#$ is the standard free energy of activation for the r.d.s.; accordingly a generalized expression for J_0 reducing to Equation A5 or A6 becomes:

$$J_0 = \bar{K}_0 c_g''\exp-\beta(\bar{\alpha}\varepsilon_0 + \Delta G_0^\#) \qquad (A7)$$

and the overall current density for reaction 7 reduces to:

$$J = 4j = J_0[\exp(-\bar{\alpha}\beta\eta_a) - \exp(4-\bar{\alpha})\beta\eta_a] \qquad (A8)$$

with the charge transfer overpotential $\eta_a = \Delta\phi - \Delta\phi_0$.

The charge transfer polarization resistance at low fields ($J\to 0$) is obtained by differentiation of Equation A8:

$$R_p = \left|\frac{\partial\eta_a}{\partial I}\right|_{J\to 0} = \frac{1}{4\beta(\pi R^2 J_0)} \qquad (A9)$$

with πR^2 the geometrical (circular) area of reaction. It has been shown by Vetter [16] that if mass transfer additionally contributes, the polarization resistance is modified to

$$R_p = \frac{1}{4\beta\pi R^2}\left(\frac{1}{J_0} + \frac{1}{J_L}\right) \qquad (A10)$$

with J_L the mass transfer limited current density.

Appendix B

Development of a theoretical model for the approach to the rate limit

Consider the overall reaction 7 in the approach to the rate-limiting state, and propose that an as yet undefined oxygen species is 'adsorbed' (through surface exchange at the gas-interface annulus) onto the mobile interfacial layer. This is followed by a combined partial charge transfer and vacancy neutralization reaction steps at a chemisorption site. The rate of adsorption at the annulus of radius R is assumed proportional to the difference in chemical activity between an oxygen species of concentration c_O on the gas side of the adsorption plane, and the mobile interfacial species of concentration c_R:

$$\gamma(c_O - c_R) = D\left|\frac{\partial c_r}{\partial r}\right|_R \qquad (B1)$$

where γ is a surface exchange coefficient and $|\partial c_r/\partial r|_R$ refers to the radial concentration gradient of the diffusing species just within the annulus. Both γ and the diffusion coefficient D are assumed to be independent of concentration. It will be noted that exchange and diffusion are sequential reactions; the slowest limiting the overall reaction rate.

Despite the destruction of the low field equilibrium between the chemisorption steps 7c'–d' and the r.d.s. 7a' by an intervening mass transfer limiting step, chemisorption of the mobile species onto the electrolyte is still likely to be fast relative to the mass transfer step. Consequently the partial reaction current density j_r at radius r can be written as the difference between the recombination and generation rates of the interfacial diffusing species at the chemisorption site of radius r:

$$j_r = 2e\,(U_r - G_r)$$

The recombination rate U_r is assumed to depend only on the concentration c_r of the diffusing species and not to require specific knowledge of the chemisorbed state. Noting that the experimental Equation 4 points to a charge transfer r.d.s. controlling the interfacial reaction even under rate-limiting conditions, Equation A8 can be modified for non-equilibrium conditions to give:

$$j_r = J_{0r}\left(\frac{c_r}{\bar{c}_r}\exp(-\alpha'_r\beta\eta_r) - \exp(1-\alpha'_r)\beta\eta_r\right) \qquad (B2)$$

The reaction transfer coefficient α'_r and over-

potential η_r include the influence of concentration overpotential as in Equation 5, and the reaction exchange current density J_{0r} corresponds to an equilibrium interfacial concentration $\bar{c}_r$.

Applying the steady state continuity equation to an elemental volume $2\pi rhdr$ of interface of height h:

$$(2\pi rhdr)\frac{\partial c_r}{\partial t} = 0 = (2\pi rhdr)D\,\nabla^2 c_r - (2\pi rdr)\frac{j_r}{2e}$$

Putting

$$K_1 = \frac{J_{0r}}{2ehD\bar{c}_r}\exp -\alpha_r'\beta\eta_r,$$

$$K_2 = \frac{J_{0r}}{2ehD}\exp(1-\alpha_r')\beta\eta_r$$

and writing in cylindrical co-ordinates,

$$\frac{1}{r}\cdot\frac{\partial}{\partial r}\left(r\frac{\partial c_r}{\partial r}\right) - K_1 c_r + K_2 = 0 \qquad \text{(B3)}$$

which is subject to the boundary conditions

$$\frac{\partial c_r}{\partial r} = 0 \text{ (symmetry at centre of interface)} \qquad \text{(B4)}$$

and

$$\gamma(c_O - c_R) = D\left|\frac{\partial c_r}{\partial r}\right|_R \qquad \text{(B1a)}$$

At equilibrium with no nett cathodic reaction, $j_r = 0$ and Equation B3 reduces to $\nabla^2 c_r = 0$ having the solution $c_r = \bar{c}_r = \bar{c}_O$ for all r. The general solution to Equation B3 satisfying the boundary condition, Equation B4 is [27]:

$$c_r = AI_0(z) + \frac{K_2}{K_1}$$

where $I_0(z)$ is the zero order modified Bessel function of argument $z = K_1^{\frac{1}{2}}r$. The derivation of A follows from boundary condition Equation B1a, and remembering $K_2/K_1 = \bar{c}_O \exp \beta\eta_r$, results in:

$$c_r = \frac{\bar{c}_O\left(\frac{c_O}{\bar{c}_O} - \exp\beta\eta_r\right)}{I_0(Z) + \frac{DZ}{\gamma R}I_1(Z)}\cdot I_0(z) + \bar{c}_O \exp\beta\eta_r \qquad \text{(B5)}$$

where $Z = K_1^{\frac{1}{2}}R$.

The total interfacial reaction current is:

$$I_r = \int_0^R 2\pi r j_r dr =$$

$$\frac{2\pi R^2 J_{0r}\left(\frac{c_O}{\bar{c}_O} - \exp\beta\bar{\eta}_r\right)I_1(Z)}{Z\left[I_0(Z) + \frac{DZ}{\gamma R}I_1(Z)\right]}\cdot\exp -\alpha_r'\beta\bar{\eta}_r \qquad \text{(B6)}$$

where $\bar{\eta}_r$ is averaged. Dividing through by $I_0(Z)$, writing $\delta = \frac{DZ}{\gamma R}\frac{I_1(Z)}{I_0(Z)}$ and noting $Z^2 = K_1R^2 = \frac{J_{0r}R^2}{2ehD\bar{c}_O}\cdot\exp(-\alpha_r'\beta\bar{\eta}_r)$, this reduces to:

$$I_r = 2\pi Rh(2e)\gamma c_O\left(1 - \frac{\bar{c}_O}{c_O}\exp\beta\bar{\eta}_r\right)\cdot\frac{\delta}{1+\delta} \qquad \text{(B6a)}$$

Considering now the surface exchange boundary at R; the exchange current across the annulus is, from Equation B1,

$$I(=I_r) = 2\pi Rh(2e)\gamma(c_O - c_R) \qquad \text{(B7)}$$

from which:

$$c_R = c_O\left(1 - \frac{I}{2\pi Rh(2e)\gamma c_O}\right) \qquad \text{(B8)}$$

But from Equation B5:

$$c_R = c_O\left(\frac{1 - \frac{\bar{c}_O}{c_O}\exp\beta\bar{\eta}_r}{1+\delta}\right) + \bar{c}_O\exp\beta\bar{\eta}_r \qquad \text{(B5a)}$$

Substituting for the bracketed term into Equation B6a and using Equation B8 yields

$$I_r = 2\pi Rh(2e)\gamma c_O \times\left[1 - \left(\frac{I}{2\pi Rh(2e)\gamma c_O}\right) - \frac{\bar{c}_O}{c_O}\exp\beta\bar{\eta}_r\right]\delta$$

But by definition from Equation B7, the limiting current I_L occurs when $c_R \to 0$:

$$I_L = 2\pi Rh(2e)\gamma c_O \qquad \text{(B9)}$$

$$\text{and } I = \delta I_L\left[\left(1 - \frac{I}{I_L}\right) - \frac{\bar{c}_O}{c_O}\exp\beta\bar{\eta}_r\right] \qquad \text{(B10)}$$

which is a general result.

Examining the nature of δ as a function of Z; for $Z \leqslant 1$, $I_0(Z) \approx 1$, $I_1(Z) \approx \frac{Z}{2}$ and $\delta I_L \rightarrow \frac{DI_L Z^2}{2\gamma R} = \pi R^2 J_{0r} \frac{c_O}{\bar{c}_O} \exp(-\alpha_r' \beta \bar{\eta}_r)$, consequently Equation B10 reduces to (expressing the current density per unit area of interface contact):

$$J = J_{0r}\left[\frac{c_O}{\bar{c}_O}\left(1-\frac{J}{J_L}\right)\exp(-\alpha_r' \beta \bar{\eta}_r) - \exp(1-\alpha_r')\beta\bar{\eta}_r\right]_{(Z\leqslant 1)} \quad \text{(B11a)}$$

being the classical electrochemical equation for the approach to the concentration limit coupled with strong activation (small J_{0r}).

On the other hand, for $Z \geqslant 10$, $I_1(Z) \sim I_0(Z)$ and $\delta I_L \rightarrow DZI_L/\gamma R$;

$$J = \left(\frac{J_{0r} J_L^2 D}{2e\gamma^2 h \bar{c}_O}\right)^{\frac{1}{2}} \times\left[\left(1-\frac{J}{J_L}\right)\exp\left(-\frac{\alpha_r'}{2}\beta\bar{\eta}_r\right) - \exp\left(1-\frac{\alpha_r'}{2}\right)\beta\bar{\eta}_r\right]_{(Z\geqslant 10)} \quad \text{(B11b)}$$

In either case the generic equation at large overpotentials (negative for a cathodic reaction) reduces to the form of equation 4:

$$|\bar{\eta}_r| = \frac{1}{\alpha_r'\beta}\left[\ln\left(\frac{J}{J_L - J}\right) + \ln\frac{J_L}{H}\right] \quad \text{(B11c)}$$

where

$$\bar{\alpha}_r' = \alpha_r', \; H = J_{0r}\frac{c_O}{\bar{c}_O} \text{ for } Z \leqslant 1$$

$$\bar{\alpha}_r' = \frac{\alpha_r'}{2}, \; H = \left(\frac{J_{0r} J_L^2 D}{2e\gamma^2 h \bar{c}_O}\right)^{\frac{1}{2}} \text{ for } Z \geqslant 10.$$

Acknowledgement

The permission of IRD to publish is acknowledged.

References

[1] J. L. Weininger and P. D. Zemany, *J. Chem. Phys.*, **22** (1954) 1469.
[2] M. Jacquin *et al.*, *C.R. Acad. Sci., Paris*, **264** (1967) 2101.
[3] T. H. Etsell and S. N. Flengas, *J. Electrochem. Soc.*, **118** (1971) 1890.
[4] R. J. Brook, W. L. Pelzmann and F. A. Kroger, *J. Electrochem. Soc.*, **118** (1971) 185.
[5] M. V. Perfilev and S. F. Palguev, *Electrochemistry of Molten & Solid Electrolytes*, **4** (1967) 147.
[6] J. E. Bauerle, *J. Phys. Chem. Solids*, **30** (1969) 2657.
[7] S. V. Karpachev and Y. M. Ovchinnikov, *Sov. Electrochem.*, **5** (1969) 181.
[8] M. Kleitz, Thesis, Grenoble University (1968).
[9] H. Yanagida, R. J. Brook and F. A. Kroger, *J. Electrochem. Soc.*, **117** (1970) 593.
[10] C. S. Tedmon, H. S. Spacil and S. P. Mitoff, *J. Electrochem. Soc.*, 116 (1969) 1170.
[11] Y. P. Gokhshstein and A. A. Safonov, *High Temp.*, **8** (1970) 368.
[12] R. E. W. Casselton, 'Electricity from MHD' *IAEA Vienna*, **5** (1968) 2951.
[13] R. E. W. Casselton, *Phys. Stat. Sol. (a)*, **2** (1970) 571.
[14] R. E. W. Casselton and M. D. S. Watson, *Sci. Ceram.*, **4** (1968) 349.
[15] R. E. W. Casselton, Thesis, University of London (1971).
[16] K. J. Vetter, 'Electrochemical Kinetics', Academic Press, New York (1967).
[17] L. R. Velho and R. W. Bartlett, *Met. Trans.*, **3** (1972) 65.
[18] L. A. Simpson and R. E. Carter, *J. Amer. Ceram. Soc.*, **49** (1966) 139.
[19] G. C. Fryburg, and H. M. Petrus, *J. Electrochem. Soc.*, **108** (1961) 496.
[20] C. A. Krier and R. I. Jaffee, *J. Less Comm. Metals*, **5** (1963) 411.
[21] J. Fusy *et al.*, *J. Chim. Phys.*, **65** (1968) 1192.
[22] T. Smith, *J. Electrochem. Soc.*, **112** (1965) 560.
[23] J. O.'M. Bockris and A. K. N. Reddy, 'Modern Electrochemistry', Macdonald, Vol. 2 (1970).
[24] M. Gideoni and M. Steinberg, *J. Sol. State Chem.*, **4** (1972) 370.
[25] R. L. Nelson, J. W. Hale and B. J. Harmsworth, *Trans. Faraday Soc.*, **67** (1971) 1164.
[26] D. Inman, Proceedings of a Symposium on 'Electromotive Force Measurements in High Temperature Systems', *Inst. Mining Metall.* (1968) 163.
[27] H. S. Carslaw and J. C. Jaeger, 'Conduction of Heat in Solids', O.U.P., 2nd Edition (1959) 192.
[28] Janaf Thermochemical Data, U.S. Dept. Comm., (1965).
[29] S. V. Karpachev and A. T. Filyaev, *Electrochem.*, **2** (1966) 1330.
[30] D. A. Wright, J. S. Thorp, A. Aypar and H. P. Buckley, *J. Mater. Sci.*, **8** (1973) 876.
[31] A. B. Lidiard, 'Handbuch der Physik', Springer Verlag, **20** (1957) 319.
[32] J. G. Simmons, *J. Phys. D.*, **4** (1971) 613.
[33] J. R. MacDonald, *J. Chem. Phys.*, **22** (1954) 1217.
[34] J. S. Thorp, Private communication.
[35] Smithsonian Physical Tables, NBS (1959).
[36] G. Cardon, *Physica*, **27** (1961) 841.
[37] J. L. Hartke, *Phys. Rev.*, **125** (1962) 1177.
[38] A. Rose, *Phys. Rev.*, **97** (1955) 1538.
[39] M. A. Lampert, *Phys. Rev.*, **103** (1956) 1648.
[40] R. E. W. Casselton, J. S. Thorp and D. A. Wright, *Proc. Brit. Ceram. Soc.*, **19** (1971) 265.

[41] W. Jakubowski and D. H. Whitmore, *J. Amer. Ceram. Soc.*, **54** (1971) 161.
[42] R. E. W. Casselton, J. Penney and M. J. Reynolds, *Trans. and J. Brit. Ceram. Soc.*, **70** (1971) 115.
[43] J. S. Thorp, A. Aypar and J. S. Ross, *J. Mater. Sci.*, **7** (1972) 729.
[44] A. Wilcockson and R. E. W. Casselton, *J. Amer. Ceram. Soc.*, **53** (1970) 293.
[45] R. C. Carter and W. L. Roth, in reference (26) p. 125.
[46] F. A. Kroger, *J. Electrochem. Soc.*, **120** (1973) 75.